Brazilian Journal of Geophysics, **42** (2024), 2, 1–14
Brazilian Geophysical Society
ISSN 2764-8044
DOI 10.22564/brjg.v42i2.2320

USING AIRBORNE MAGNETIC AND RADIOMETRIC DATA TO UNRAVEL AURIFEROUS PROSPECTIVE AREAS IN THE PITANGUI GREENSTONE BELT, NW OF QUADRILÁTERO FERRÍFERO – MG, BRAZIL

Brener Otávio Luiz Ribeiro [1*], Danilo Barbuena [1], and Gustavo Henrique Coelho de Melo [2]

[1]Universidade Federal dos Vales do Jequitinhonha e Mucuri, LESTE, Diamantina, MG, Brazil
[2]Universidade Federal de Ouro Preto – UFOP, Ouro Preto, MG, Brazil

*Corresponding author: brener.ribeiro@ufvjm.edu.br

ABSTRACT. The Pitangui Greenstone Belt (PGB), NW of the Quadrilátero Ferrífero, Brazil, is a metavolcano-sedimentary sequence that hosts some important gold deposits recently discovered. Research has been made in the PGB to understand its gold mineral system, but the information regarding the prospective vectors associated with gold mineralization is still unclear. Here, we show the application of airborne magnetic and radiometric data to find the spatial relation between hydrothermal alteration zones and the structural framework of the PGB region. The results showed that the occurrence of gold deposits is associated with NW-SE structures and hydrothermal alteration zones. This association does not exist with E-W structures, which has direct implications on the relevance of these structures in the prospective modeling. Additionally, the application of radiometric data to map hydrothermal alteration zones showed that the limitations of this technique can generate anomalies not strictly associated with hydrothermal processes. In this case, some anomalies could be linked with secondary processes like weathering, leaching, transportation and accumulation of mobile elements, such as K and U.

Keywords: airborne geophysical data, hydrothermal alteration mapping, geophysical-structural mapping, gold exploration.

INTRODUCTION

The discovery of new mineral deposits has declined over the last few decades as the new ore findings have become increasingly smaller, deeper, geologically more complex and sited in more remote areas (Dentith and Mudge, 2014; McCuaig and Hronsky, 2014; Schodde, 2017). This means that undiscovered primary and secondary dispersion halos and geological structures related to mineralization (i.e., footprints) are proportionally restricted, turning the identification of mineral deposits a difficult task.

In this scenario, prospective models capable of identifying small-scale mineralization have been one of the focuses of exploration research. Therefore, several advances to create evidential maps (EM) were achieved over the years. EMs are maps of geological features strictly related to mineral deposits, such as structural framework, geochemical signatures, geophysical anomalies, hydrothermal alteration halos and units favorable to host mineralization (Crosta et al., 2003; Leite and de Souza Filho, 2009; McCuaig et al., 2010; Czarnota et al., 2010; McCuaig and Hronsky, 2014; Hagemann et al., 2016). These maps can indicate the occurrence of mineralized zones, within different geological settings, and can be used to create mineral prospectivity models (MPMs) (Bonham-Carter, 1994; Harris et al., 2001).

Gold deposits hosted in greenstone belt sequences are formed at depths ranging from 2 to 15 km, involving fluids from different sources (Goldfarb and Groves, 2015; Groves et al., 2020). These deposits exhibit regional prospective guides that include: i)

regional-scale structures that operate as pathways for hydrothermal fluids and control the mineralization; ii) specific host rocks (e.g., banded iron formations); iii) zones of hydrothermal alteration associated with regional structures and iv) geochemical footprints of ore formation (Bierlein et al., 2006; Herbert et al., 2014; Ford et al., 2019; Groves et al., 2020).

In mineral exploration, airborne geophysical data have been used as an efficient tool to map structures and hydrothermal alteration zones that may be linked to mineralization (Carrino et al., 2007; Souza Filho et al., 2007; Barbuena et al., 2013). This procedure is applied particularly in greenfield exploration areas for regional characterization (Holden et al., 2012; Barbuena et al., 2013; Ribeiro et al., 2014; Couto et al., 2016).

Thus, magnetic and radiometric data became one of the greatest supports for mineral exploration. The former provides information about structures and magnetic bodies at deeper crustal levels, whereas the latter can reveal the main lithological domains and identify hydrothermal alteration zones (Ribeiro et al., 2014; Ribeiro and Mantovani, 2016; Campos et al., 2017; Cunha et al., 2017). Together, they can work as a powerful tool in identifying mappable expressions for prospective models.

Recent studies indicate that the Pitangui Greenstone Belt (PGB) has great potential to host gold mineralization due to similarities with the Quadrilátero Ferrífero (QFe) region, particularly regarding its geological and metallogenic setting (e.g., Lobato et al., 2001b,a; Romano et al., 2013; Tassinari et al., 2015; Soares et al., 2017, 2018; Ribeiro et al., 2023). However, the PGB region still lacks more detailed studies focused on prospective vectors that can indicate favorable targets for gold mineralization.

This research had as its main objectives: i) characterize the region structural framework, in surface and subsurface, by processing and interpreting aeromagnetic data, ii) identify zones of hydrothermal alteration through radiometric data, iii) support prospective studies in the PGB region, and iv) contribute to the knowledge of the PGB gold exploration potential by understanding its main prospective vectors.

GEOLOGICAL SETTING

The PGB is located northwest of the Quadrilátero Ferrífero (QFe), São Francisco Craton, and consists of an Archean sequence deposited in an oceanic basin, during the Rio das Velhas I (2.93 – 2.85 Ga) and II (2.80 – 2.76 Ga) events (Lana et al., 2013; Farina et al., 2015; Soares et al., 2017, 2020). This sequence is subdivided into two main units: the Pitangui Group and the Antimes Formation (Marinho et al., 2018, 2023). The Pitangui Group is composed of metaultramafic, metamafic and intermediate metavolcanic rocks interspersed with metasedimentary rocks, such as schists, metacherts and metabanded iron formations. The Antimes Formation, on the other hand, is composed of quartzites and metaconglomerates (Soares et al., 2017; Marinho et al., 2018, 2023).

The rocks were metamorphosed into greenschist to amphibolite facies and intruded by medium to high-K granitoids, emplaced at the end of the Rio das Velhas orogeny (2.76 – 2.68) (Farina et al., 2016; Soares et al., 2020).

The PGB has a synclinorium architecture oriented in the NW-SE direction, bordered by Meso to Neoarchean TTG complexes, and it is partially covered by Paleoproterozoic, Neoproterozoic and Phanerozoic supracrustal sequences. The region also presents mafic dyke swarms that cross-cut Archean and Paleoproterozoic units (Soares et al., 2017, 2018, 2020; Marinho et al., 2018, 2023, Figure 1).

The main regional structures trend in the NW-SE direction and the anastomosed NW-SE lineaments mark the suture of the PGB with the Divinópolis and Belo Horizonte - Bonfim blocks during the Rio das Velhas orogeny (Romano et al., 2013; Soares et al., 2020).

The E-W strike-slip structures, however, were generated during the NW thrusting of the Serra do Curral nappe, where the Minas and the Estrada Real Supergroup outcrops, in the Rhyacian-Orosirian orogeny. This tectonic event was also responsible for reactivating Archean NW-SE structures (Figure 1) and probably for overprinting the gold mineralization (Endo and Chamale Júnior, 1992; Hartmann et al., 2006; Romano et al., 2013; Koglin et al., 2014; Dopico et al., 2017).

Gold deposits in the Pitangui Greenstone Belt and its prospective guides

Gold in the PGB deposits occur in sulfide assemblages in quartz-carbonate veins, that are structurally controlled by shear zones (e.g., Turmalina and Pitangui deposits), or strata confined in banded iron formations (São Sebastião deposit) (Soares et al., 2018; Fabricio-Silva et al., 2019; Maurer et al., 2021). The mineralization occurs mainly hosted in mafic, metavolcaniclastic meta-volcanic and metasedimentary rocks, along regional NW-SE shear zones, particularly in the Pitangui and Onça-Penha lineaments (Fabricio-Silva et al., 2019; Maurer et al., 2021).

Hydrothermal alteration zones are restricted, extending no more than 100 meters from the mineralization, and present sericite, chlorite, carbonate and tourmaline on the alteration halos (Soares et al., 2018; Fabricio-Silva et al., 2019; Maurer et al., 2021). These zones envelop the main gold-bearing lodes that present a great variety of sulfides (Soares et al., 2018; Fabricio-Silva et al., 2019).

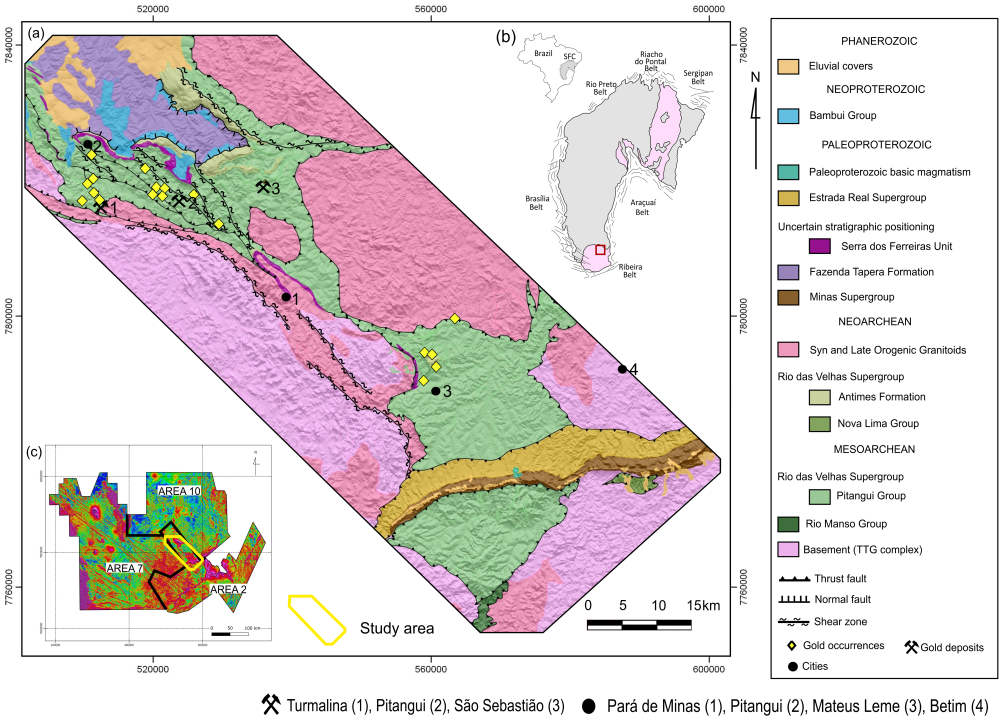

Figure 1: (a) Geological map of the study area. (b) Subdivision of the São Francisco Craton (Archean-Paleoproterozoic basement in pink). (c) Analytical Signal of the Residual Magnetic Field (RMF) with limits of the aerogeophysical survey projects that cover the study area. Adapted from: Romano (2007); Romano et al. (2009, 2013); Ribeiro and Baltazar (2013); Braga et al. (2013); Marinho et al. (2018); Silva et al. (2020)

The timing of mineralization is still controversial. Geological features, including structural control, mineralization style and similarities with gold deposits of the QFe suggest that mineralization was likely formed during the Archean (Fabricio-Silva et al., 2019, 2021). However, recent research (e.g., Tassinari et al., 2015; Soares et al., 2021) points to ages of 2.0 – 1.9 Ga, which suggests an overprint of the gold mineralization, possibly caused by the reactivation of Archean structures during the Rhyacian-Orosirian orogeny (Soares et al., 2021).

In this context, the main prospective guides for deposits in the PGB region that can be detected from the interpretation of airborne geophysical data include (i) regional structures that may have worked as pathways for mineralized fluids and (ii) halos of hydrothermal alteration, as an expression of the reactions between fluids and host rocks. Both of these features are entangled, presenting a spatial relation and, therefore, indicating regions that are more likely to host gold mineralization.

MATERIALS AND METHODS

The study was conducted using: (i) the airborne geophysical surveys acquired by the Minas Gerais Economic Development Company (CODEMIG), from Areas 2, 7 and 10 (Table 1); (ii) the Digital Elevation Model (DEM) from the ALOS PALSAR sensor, with a spatial resolution of 12.5 meters; and (iii) the geological mapping data of the PGB region (Romano, 2007; Braga et al., 2013; Romano et al., 2013; Ribeiro and Baltazar, 2013; Marinho et al., 2018; Silva et al., 2020).

Airborne magnetic data

The airborne magnetic data were used to identify magnetic lineaments that could be associated with geological structures on the subsurface. The data processing was carried out using the reduced magnetic field for the International Geomagnetic Reference Field (IGRF) as a basis for the application of enhancement operations. The data were interpolated using the bidirectional method, with a cell size of 125 meters, $\frac{1}{4}$ of the flight lines spacing of the project with the lowest resolution, Area 10 - Belo Horizonte - Curvelo - Três Marias (Table 1). The data from each project were processed individually and the final grid products were merged.

The Fourier filters used in this study include: (i) Analytical Signal Amplitude (ASA); (ii) Tilt Derivative (TDR) and (iii) Vertical Gradient (Dz) (Evjen, 1936; **?**; Blakely, 1996). The x, y and z derivatives of the residual magnetic field, Dx $\left(\frac{\partial M}{\partial x}\right)$, Dy $\left(\frac{\partial M}{\partial y}\right)$ and Dz $\left(\frac{\partial M}{\partial z}\right)$, respectively, have the function of boosting the high frequencies of points aligned in their respective directions, where M represents the Magnetic Field reduced to IGRF (Cordell and Grauch, 1985).

Table 1: Parameters of the airborne geophysical surveys of areas 2, 7 and 10.

Parameters	**Area 2 Pitangui – São João Del Rei – Ipatinga**	**Area 7 Patos de Minas – Araxá – Divinópolis**	**Area 10 Belo Horizonte – Curvelo – Três Marias**
Flight line direction	N30E (West block), N30W (East block)	NS	NS
Flight line spacing	250 m	400 m	500 m
Control line direction	N60W (West block), N60E (East block)	EW	EW
Control line spacing	2 500 m	8 000 m	10 000 m
Interval between consecutive geophysical measurements	0.1 s (magnetometer), 1.0 s (spectrometer)	0.05 s (magnetometer), 1.0 s (spectrometer)	0.1 s (magnetometer), 1.0 s (spectrometer)
Average flight height	100 m	100 m	100 m
Approximate flight speed	200 km/h	280 km/h	270 km/h
Year of survey	2001	2006	2008/2009
Company	LASA Engineering and Prospections S.A	LASA Engineering and Prospections S.A	CODEMIG and Brazilian Geological Survey

The ASA corresponds to the magnitude of the gradient vector and calculates the maximum amplitude of the anomaly and centralizes it over the source, regardless of the variation direction. Shallow sources exhibit more intense anomalies, while deeper sources display more smooth anomalies (Equation 1; Nabighian, 1972, 1974; Roest et al., 1992).

$$ASA = \sqrt{\left[\left(\frac{\partial M}{\partial x}\right)^2 + \left(\frac{\partial M}{\partial y}\right)^2 + \left(\frac{\partial M}{\partial z}\right)^2\right]}, \quad (1)$$

The TDR (θ) allows the identification of magnetic lineaments that delimit bodies, intrusions, faults and fractures through anomaly direction (Equation 2; Miller and Singh, 1994). This operation has greater stability with less variation when compared to ASA. Thus, the TDR is more suitable for ascertaining the extent and direction of sources, especially geological structures not highlighted by the ASA method (Miller and Singh, 1994). All products mentioned above were interpreted together with the mapped structures from the geological maps and the DEM, resulting in a geophysical-structural map containing all surface and subsurface regional lineaments.

$$\theta = \left[\frac{\frac{\partial M}{\partial z}}{\frac{\partial M}{\partial h}}\right], \quad (2)$$

Where:

$$\frac{\partial M}{\partial h} = \sqrt{\left[\left(\frac{\partial M}{\partial x}\right)^2 + \left(\frac{\partial M}{\partial y}\right)^2\right]}, \quad (3)$$

Airborne radiometric data

The airborne radiometric data were used to create maps capable of identifying zones of hydrothermal alteration. The procedure aimed to highlight regions enriched in potassium and/or uranium – mobile elements that can be remobilized by hydrothermal fluids – in comparison with thorium concentration, which has lower mobility. The techniques used here were: (i) K/Th ratio (KeTh); (ii) F parameter (Equation 4) (iii) anomalous K (Kd; Equation 5); and (iv) anomalous U (Ud; Equation 6).

$$FParameter = k\frac{eU}{eTh}, \quad (4)$$

$$K_d = \frac{(K - K_i)}{K_i}; K_i = Th\frac{\overline{K}}{\overline{Th}}, \quad (5)$$

$$U_d = \frac{(U - U_i)}{U_i}; U_i = Th\frac{\overline{U}}{\overline{Th}}, \quad (6)$$

Where K_i and U_i correspond to the ideal values of K and U, while $\overline{K}$, $\overline{Th}$ and $\overline{U}$ consists of the average concentrations of the radionuclides.

The K/Th ratio shows the concentration of K compared to Th, while the F parameter shows the enrichment of K and U compared to Th (Ferreira, 1991; Barbuena et al., 2013; Campos et al., 2017). K_d and U_d are based on the same principle: the calculation of ideal values for each sampling point. These ideal values are used as parameters and the deviations above or below these parameters correspond to K and U anomalies (Pires, 1995).

After creating the four maps, the Principal Component Analysis (PCA) was performed to search for a principal component (PC) that best controls the data variability. The PC that positively controls all four radiometric maps was chosen to represent hydrothermal alteration zones. The map of geological-geophysical lineaments was analyzed together with the map of hydrothermal alteration zones and the location of known deposits and occurrences to understand the spatial relation between these features and how good they can be in mapping prospective zones.

RESULTS

Geophysical-structural mapping

The aeromagnetic data were used to create maps that highlight magnetic structures, such as ASA, TDR and Dz. These products were interpreted together with the mapped structures from the geological map and the DEM (Figure 2a). Four structural domains were identified, in addition to several unmapped magnetic and relief lineaments (Figures 3 and 4). The TDR and Dz images allowed the identification of four geophysical-structural domains with a predominant pattern in the NW-SE direction (Figure 4).

In comparison to the geological map (Figure 1a), these domains coincide with lithologies that display different rheological behavior. Domain I corresponds to sinuous, anastomosed and continuous lineaments that coincide with the region where the greenstone belt rocks outcrop (Figure 4b).

Domain II, however, displays linear, extensive and conjugated structures in granite-gneissic terrains. The conjugate lineaments are arranged in the NNW-SSE and WNW-ESE directions (Figure 4c).

Domain III encompasses the meta-sedimentary package that covers the PGB in the northwest portion of the area, including the Paleoproterozoic rocks of the Fazenda Tapera Formation, the Neoproterozoic rocks of the Bambuí Group and the Phanerozoic cover (Marinho et al., 2018). This domain is composed of linear structures of small extension, identified through TDR and Dz images, with a WNW-ESE direction (Figure 4d).

Finally, Domain IV has a low density of structures compared to domains I and II and it is dominated by linear structures of different length and directions. These structures oscillate around E-W direction, often oriented in WNW-ESE and ENE-WSW directions (Figure 4e).

Hydrothermal alteration zones

The airborne radiometric data were used in this research to detect hydrothermal alteration zones. Here, the concentrations of K, Th and U were evaluated throughout the study area (Figure 5). To obtain an interpretation from these products, the following factors were considered: i) radiometric data provides surface information up to a maximum of 40 centimeters deep; ii) techniques such as K_d and U_d are effective in regions with a certain compositional homogeneity, because these parameters are calculated using the average value of the concentrations of the radionuclides disregarding the lithotype (Equations 5 and 6). Thus, the rocks analyzed from these products must show similarity in terms of K, Th and U contents; and iii) K, Th and U-rich rocks can mask anomalies in the rocks of the greenstone belt itself, that has low contents of these three elements. Therefore, it is important to calculate the Kd and Ud parameters in groups of lithological units that have similar concentrations of the three elements.

The maps and boxplots of Figure 5 indicate low concentration values of all three radionuclides in the PGB, when compared to the adjacent radiometric domains (Figure 5). This contrast occurs due to different concentrations of K, Th and U in each unit, as each set of rocks has its own background for these three elements.

This observation should be considered in the analysis of hydrothermal alteration zones once the background values of granite-gneiss complexes are much higher than those from the greenstone belt sequences, for instance (Figure 6a). This discrepancy between values can result in products that mask the hydrothermal alteration zones in regions where the background concentrations of radionuclides are lower than their surroundings.

To reduce the effect of contrast between the lithologies and to prevent neglecting potential hydrothermal zones, the calculation of K_d and U_d was performed individually for each group indicated in the boxplots (Figure 5). The K/Th ratio and F Parameter were not calculated individually like K_d and U_d because these methods show the proportionality between the three radionuclides and, therefore, do not depend on a regional average concentration value.

All the maps that indicate possible hydrothermal alteration zones suggest intense radiometric anomalies along the PGB, particularly in the northwest sector (Figure 6). The maps also show high values in

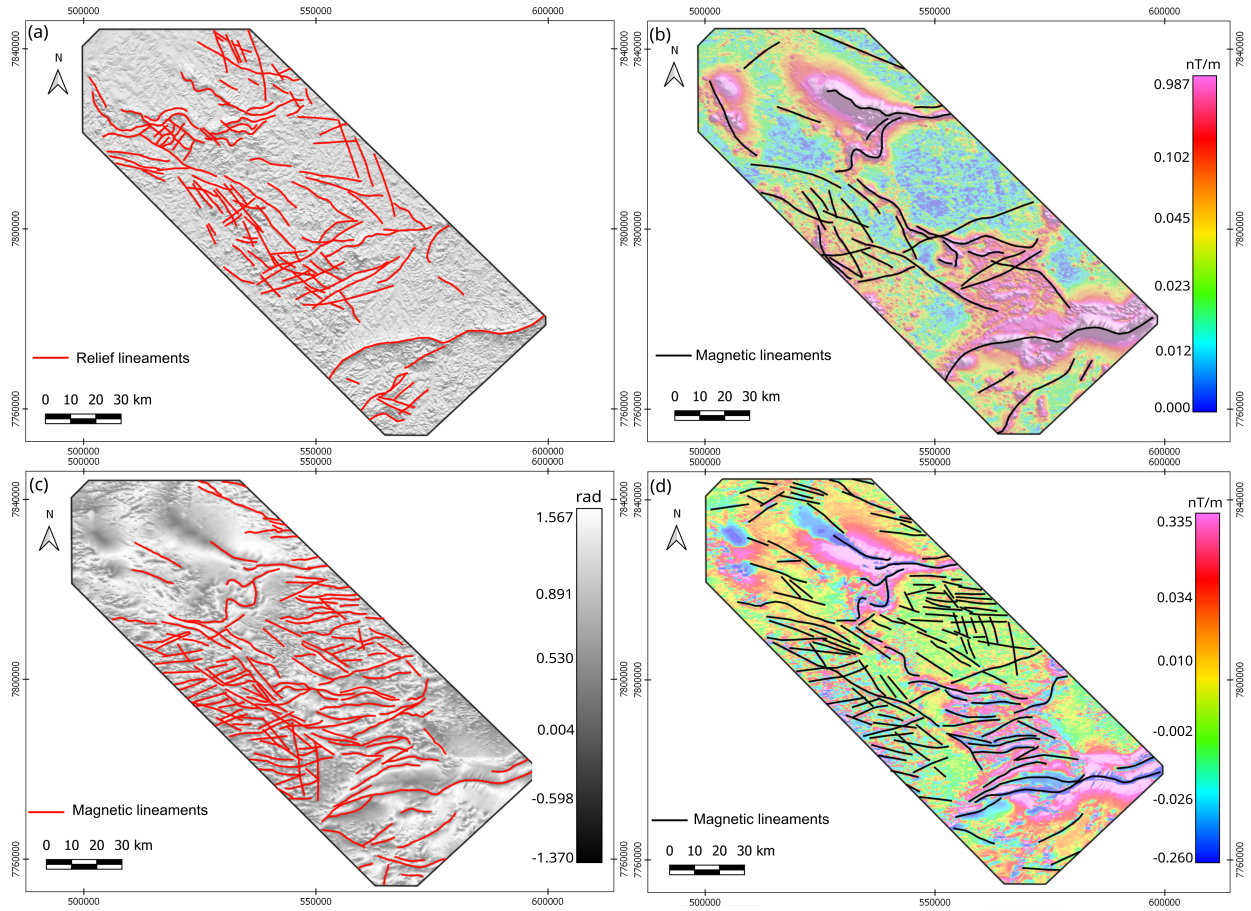

Figure 2: (a) Digital Elevation Model (DEM). (b) Map of Analytical Signal Amplitude (ASA) of the RMF. (c) Map of the Tilt Derivative (TDR) of the RMF. (d) Map of the vertical gradient (Dz) of the RMF.

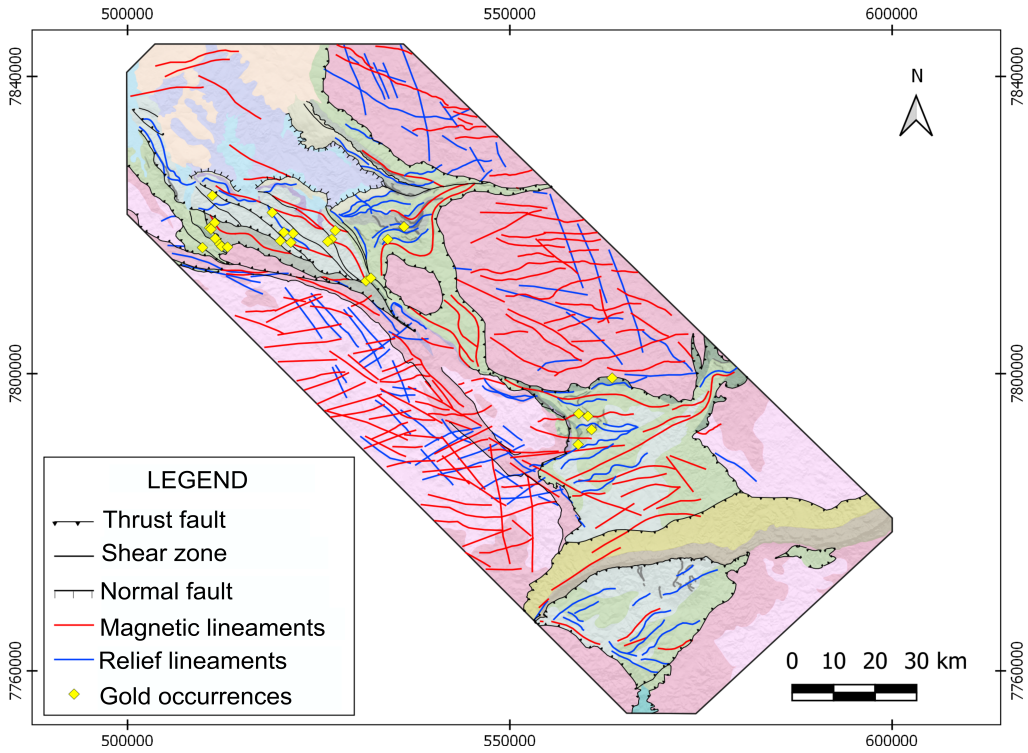

Figure 3: Map of geological-geophysical lineaments based on the interpretation of aerogeophysical data and the Digital Elevation Model (DEM).

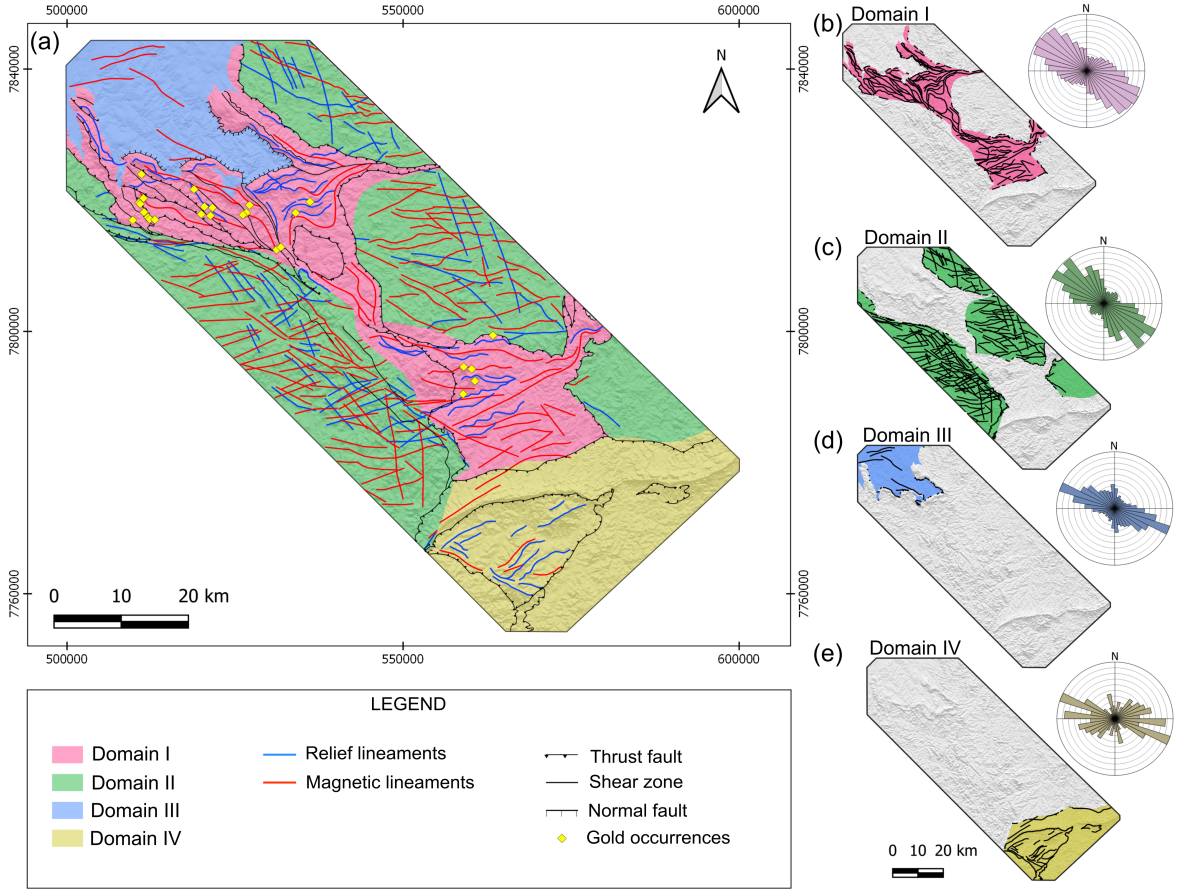

Figure 4: (a) Map of geophysical-structural domains of the study area. (b) Map of the structural domain I. (c) Map of the structural domain II. (d) Map of the structural domain III. (e) Map of the structural domain IV.

regions where Neoarchean high-K granitic bodies outcrop. The K_d and K/Th ratio maps are quite similar when compared to each other. This is because both products measure K concentrations compared to the Th contents.

The Principal Component Analysis (PCA) was used on the radiometric data to reduce the number of variables, expressing, in a single map, possible zones of hydrothermal alteration (Figure 7). The results indicate that PC1 controls the greatest variability of the data (82.9%) and strongly represents the four radiometric maps (Figure 7d). The screeplot (Figure 7c) also indicates that PC1 is the only representative PC for the database variability.

The PC1 versus PC2 diagram (Figure 7b) represents 95.6% of the data variability and shows a strong relation between F parameter and U_d, due to both products highlight the enrichment of U. Similarly, this can also be observed for K_d and the K/Th ratio, which emphasize the high concentration of K. The Figure 7a presents the scores of the representative vector (PC1) that controls the variability of K_d, U_d, F parameter and K/Th ratio. High PC1 score values indicate a high similarity between high values of the four maps, while low score values indicate a high similarity between low values of the four radiometric maps.

DISCUSSION

Geological-geophysical analysis and implications for PGB geology

Through magnetic data and DEM we observed four geophysical-structural domains spatially correlated with the main geological units of the region. These domains were recognized based on the extent, geometry and orientation of large regional structures (Figure 4).

Domain I groups sinuous and anastomosed structures in an NW-SE direction that coincide with the portion where the greenstone belt sequence outcrops. The sinuosity is associated with the rheology of the greenstone belt rocks, which have a less competent behavior compared to the granite-gneissic terrains that surround them.

There is also a slight change in the directional pattern of the structures that converge in the E-W direction between Pequi and Florestal Batholiths. This wide variation around the NW-SE direction is a response of the anastomosed pattern of the structures.

Domain II, however, has a set of conjugated structures in the NW-SE and E-W directions. These structures are rectilinear and occur in more competent rocks with brittle behavior, such as granitic bodies and TTG complexes that outcrop within the PGB

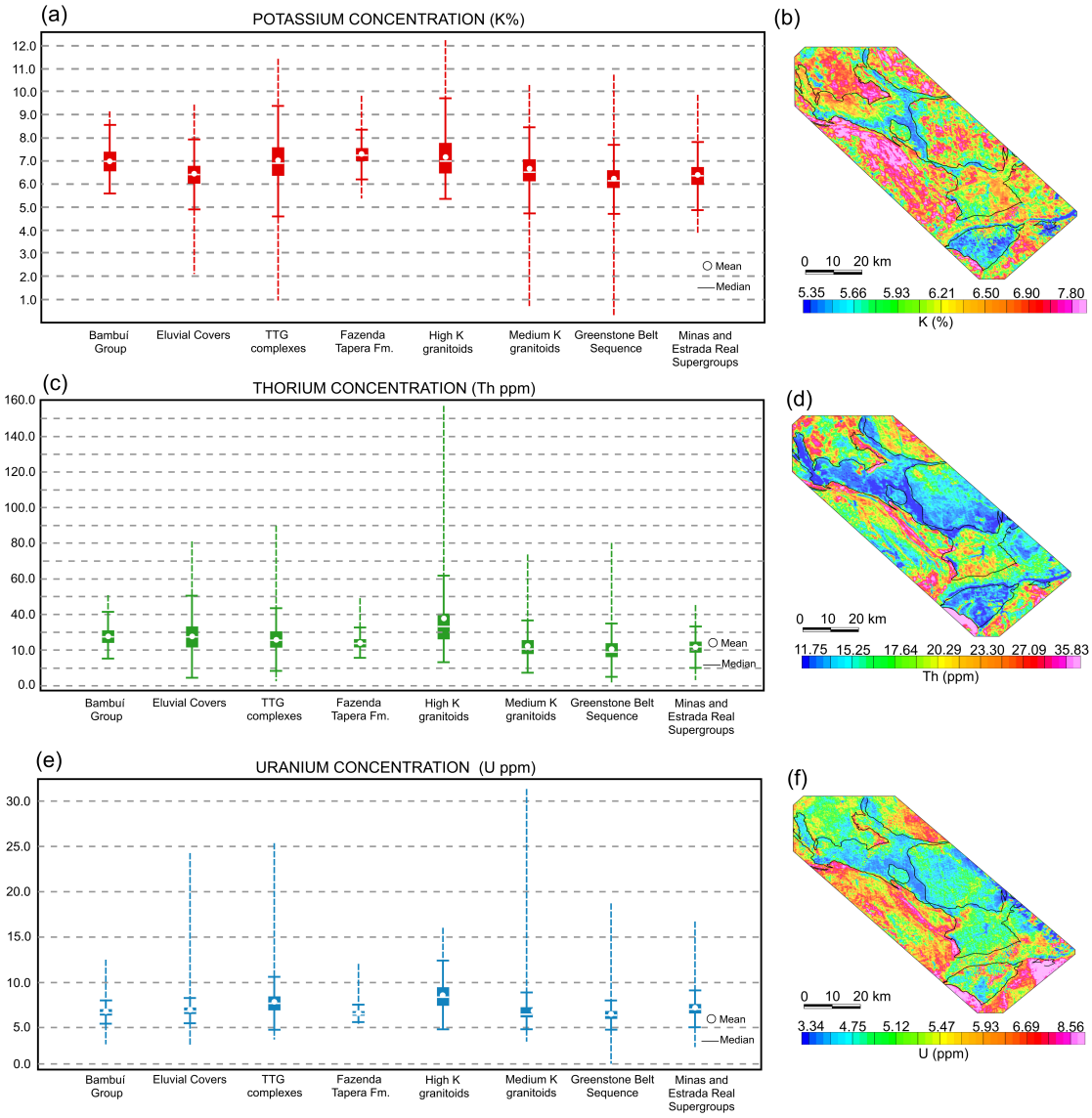

Figure 5: Boxplot graph of K, Th and U concentrations and their respective maps. (a) Boxplot of K (%) concentrations. (b) Radiometric map of the K (%) concentration. (c) Boxplot of Th (ppm) concentrations. (d) Radiometric map of the Th (ppm) concentration. (e) Boxplot of U (ppm) concentrations. (f) Radiometric map of the U (ppm) concentration.

and in its surrounding areas. The predominance of NW-SE structures in these two domains, although with a slightly different geometry, may be associated with regional shear zones and axial fold traces that follow this same pattern.

These structures were likely formed during the Rio das Velhas orogeny, at ca. 2.7 Ga, reactivated during the Rhyacian-Orosirian orogeny at ca. 2.1 Ga (Fabricio-Silva et al. 2019; Soares et al. 2020, 2021) and were responsible for controlling most of the PGB gold mineralization (Fabricio-Silva et al., 2019).

Domains III and IV record a lower density of structures when compared to domains I and II. Domain III encompasses the Paleoproterozoic, Neoproterozoic and Phanerozoic units and has a NW-SE direction pattern, suggesting that those structures were inherited from the reactivation of Archean structures present in the greenstone belt sequence that probably underlie such units.

Domain IV has a low density of structures that follow an E-W direction pattern, which coincides with the Serra do Curral architecture. This pattern can be related to the thrusting of the Serra do Curral nappe that resulted in the propagation of ENE-WSW and WNW-ESE strike-slip faults in the southern portion of the PGB (Endo and Chamale Júnior, 1992; Romano et al., 2013; Endo et al., 2019).

Zones of hydrothermal alteration revealed by radiometric data

The gold deposits in the region show zones of hydrothermal alteration with sericite, chlorite, carbonate and tourmaline (Soares et al., 2018; Fabricio-Silva et al., 2019; Maurer et al., 2021). However, these halos appear to be incipient, narrow and restricted to the vicinity of the shear zones. Thus, radiometric data can reveal not exactly the halos, but only the path-

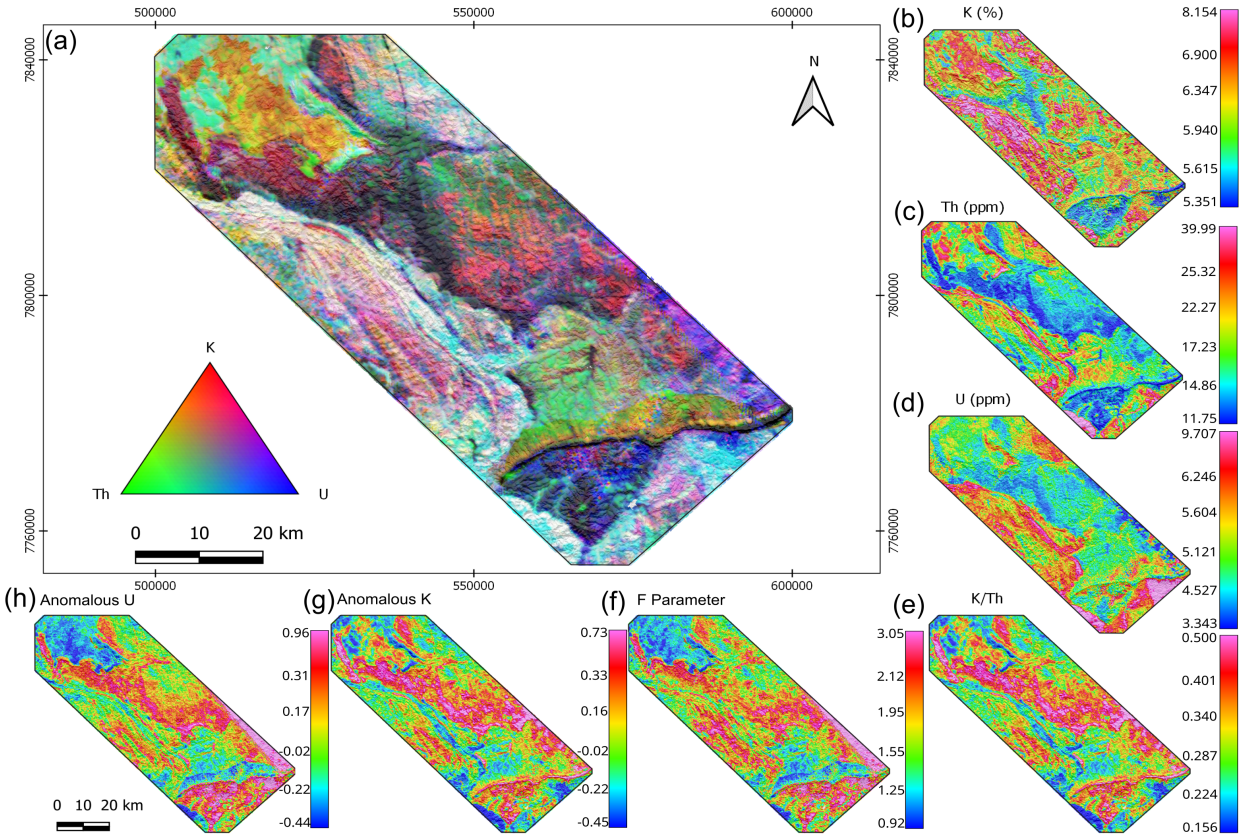

Figure 6: (a) RGB of K, Th and U ternary composition. (b) K concentration map (%). (c) Th concentration map (ppm). (d) U concentration map (ppm). (e) K/Th ratio map. (f) F Parameter map. (g) Anomalous K map (Kd). (h) Anomalous U map (Ud).

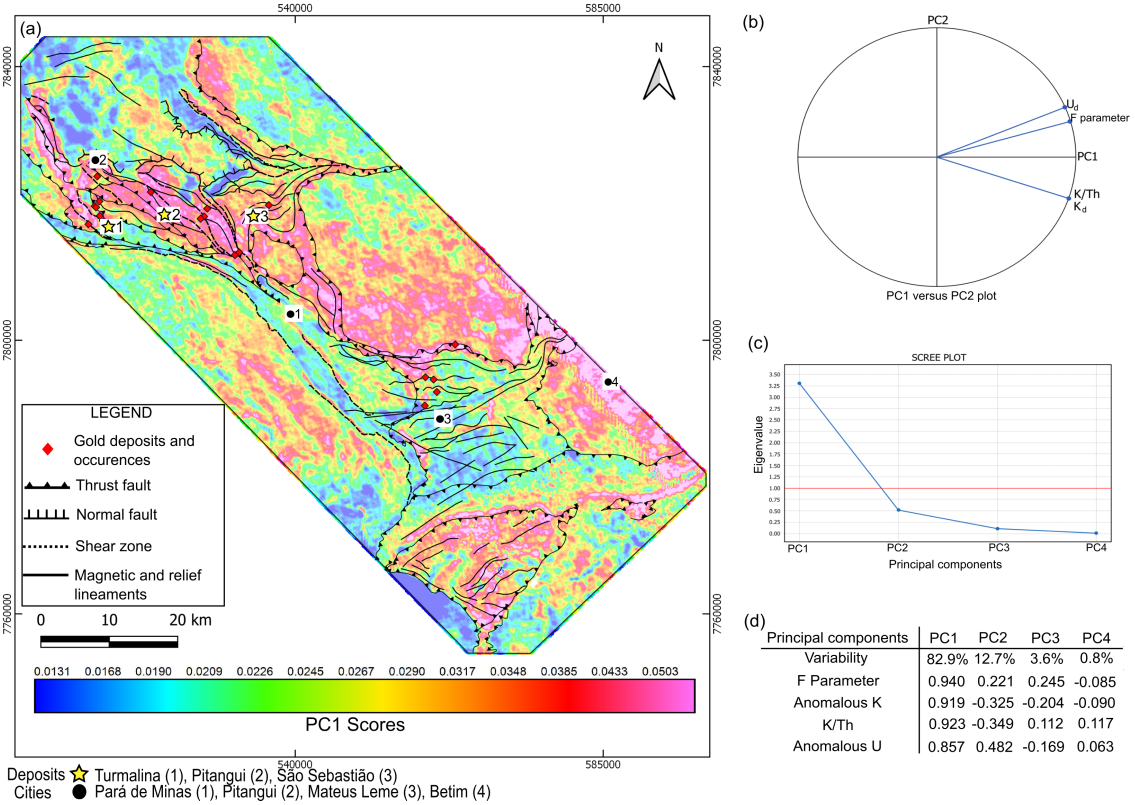

Principal components	PC1	PC2	PC3	PC4
Variability	82.9%	12.7%	3.6%	0.8%
F Parameter	0.940	0.221	0.245	-0.085
Anomalous K	0.919	-0.325	-0.204	-0.090
K/Th	0.923	-0.349	0.112	0.117
Anomalous U	0.857	0.482	-0.169	0.063

Figure 7: (a) PC1 score map. (b) PC1 versus PC2 graph. (c) Screeplot graph of the four principal components generated. (d) Table with the parameters of each principal component.

ways of hydrothermal fluids that showed variation in the three radiometric channels.

The PC1 map showed that most anomalies occur in the PGB region and are spatially associated with regional structures that may have worked as pathways of mineralized fluids. This suggests that the aligned high concentration values of K and/or U might be associated with hydrothermal alteration processes. However, some regions, such as the north of Serra do Curral and east of the Mateus Leme district (point 3 in Figure 7), have high values following a dendritic pattern. This indicates that the map also highlights high concentrations of K in alluvial deposits, promoted by surficial dynamics.

Therefore, despite the high reliability of the PCA, many interferences and anomalies not associated with hydrothermal alteration can remain in the evidential map, due to surface conditions, such as differential K leaching for alluvial deposits.

The southern portion of Serra do Curral also shows areas with high contents of the PC1 score that probably are not correlated with hydrothermal alteration zones. This region displays anomalous PC1 values, covering its entire length, not spatially associated with major regional structures, reinforcing the hypothesis that these anomalies are not linked to hydrothermal alteration and, consequently, to gold mineralization.

Airborne geophysical data as an efficient tool for gold prospecting in the PGB

The analysis of airborne geophysical data in the PGB region allowed the characterization of regional lineaments associated with zones with high probability of hydrothermal alteration or fluid passage. Most of the anomalous values of PC1 follow the Archean NW-SE structures (Romano, 2007; Fabricio-Silva et al., 2019; Soares et al., 2020).

The NE-SW and E-W structures located in the southeastern portion of the PGB, however, were probably formed by the thrusting of the Serra do Curral nappe during the Rhyacian-Orosirian orogeny and are not associated PC1 anomalies (Endo and Chamale Júnior, 1992; Romano et al., 2013; Endo et al., 2019). The absence of radiometric anomalies along these structures may be connected with the lack of expressive hydrothermal fluid circulation during the Paleoproterozoic orogeny.

This observation has direct implications for orogenic gold prospecting. Even considering the remobilization of gold during the Paleoproterozoic orogeny (Tassinari et al., 2015; Soares et al., 2021), this assumption reduces the relevance of these structures as prospective vectors for gold deposits.

Another possibility is that the absence of radiometric anomalies is related to the presence of a lateritic plateau that covers the E-W structures. As a result, the radiometric response shows great concentration of thorium compared to the other radionuclides, due to K and U leaching caused by the drainage system that flows towards northwest of the area.

The map in Figure 7 shows that the gold deposits, such as São Sebastião, Turmalina and Pitangui, are located within regions with high density of structures and high values of PC1 scores. The map also shows that the relation between structures and PC1 scores is significant only in areas where there is a large number of structures that extent until the surface, due to the limitations of the airborne radiometric technique. Therefore, this work provided insights to conclude that the airborne magnetic data aligned to radiometric data are effective in the identification of hydrothermal alteration zones and unmapped structures that can be used as proxies in MPMs.

CONCLUSIONS

Magnetometry and radiometry airborne geophysics are efficient tools for prospecting new ore deposits not only in the PGB but also in other deposits around the world that have a similar geological context. The data processing and interpretation allowed us to draw the following conclusions:

- The identified geophysical lineaments in subsurface showed a direction pattern compatible with the structural framework presented by the geological mapping of the region and complemented the knowledge regarding the structures of the PGB (i.e., Fabricio-Silva et al. (2019); Fabricio-Silva et al. (2021)).

- The PCA applied to the K/Th ratio, K_d, U_d and F parameter maps indicated that the zones with the highest score are in the PGB region, suggesting intense hydrothermal activity in the mineralization host sequence.

- There is a direct spatial relation between the occurrences and gold deposits, the high values presented by the PCA and the identified geophysical-structural lineaments, reinforcing the reliability of the hydrothermal alteration and the geophysical-structural maps.

- The regions with the highest probability to have hydrothermal alteration zones are found along the PGB and coincide with areas where there is a higher density of structures, such as in the regions of the São Sebastião, Pitangui and Turmalina deposits, reinforcing the importance of using these techniques to generate evidential maps for prospective modeling.

REFERENCES

Barbuena, D., C. R. Souza Filho, E. P. Leite, E. M. Junior, R. R. Assis, R. P. Xavier, F. J. F. Ferreira, and A. J. P. Paes de Barros, 2013, Airborne geophysical data analysis applied to geological interpretation in the alta floresta gold province, mt: Brazilian Journal of Geophysics, **31**, 169–186, doi: 10.22564/rbgf.v31i1.254.

Bierlein, F. P., D. I. Groves, R. J. Goldfarb, and B. Dubé, 2006, Lithospheric controls on the formation of provinces hosting giant orogenic gold deposits: Mineralium Deposita, **40**, 874–886, doi: 10.1007/s00126-005-0046-2.

Blakely, R. J., 1996, Potential theory in gravity and magnetic applications: Cambridge University Press.

Bonham-Carter, G. F., 1994, Geographic information systems for geoscientists: modelling with GIS, volume **13** *of* Computer Methods in the Geosciences: Elsevier.

Braga, D., O. F. Baltazar, and E. A. M. dos Santos, 2013, Carta geológica: folha Divinópolis, SF.23-X-A-I. Scale 1:100.000: CPRM – Serviço Geológico do Brasil. Ministério de Minas e Energia.

Campos, L. D., S. M. de Souza, D. A. de Sordi, F. M. Tavares, E. L. Klein, and E. C. D. S. Lopes, 2017, Predictive mapping of prospectivity in the gurupi orogenic gold belt, north–northeast Brazil: an example of district-scale mineral system approach to exploration targeting: Natural Resources Research, **26**, 509–534, doi: 10.1007/s11053-016-9320-5.

Carrino, T. A., C. R. D. Souza Filho, and E. P. Leite, 2007, Avaliação do uso de dados aerogeofísicos para mapeamento geológico e prospecção mineral em terrenos intemperizados: o exemplo de Serra Leste, província mineral de Carajás: Revista Brasileira de Geofísica, **25**, 307–320, doi: 10.1590/S0102-261X2007000300007.

Cordell, L., and V. J. S. Grauch, 1985, Mapping basement magnetization zones from aeromagnetic data in the San Juan Basin, New Mexico, *in* The Utility of Regional Gravity and Magnetic Anomaly Maps: Society of Exploration Geophysicists, 181–197. doi: 10.1190/1.0931830346.ch16.

Couto, M. A., O. F. Baltazar, R. C. R. Ferreira, M. S. Marinho, and J. C. S. Araújo, 2016, Modelagem e integração geofísica (htem, magnetometria e gamaespectrometria) no greenstone belt rio das velhas, quadrilátero ferrífero, mg: Presented at the VII Simpósio Brasileiro de Geofísica, SBGf.

Crosta, A. P., C. R. de Souza Filho, F. Azevedo, and C. Brodie, 2003, Targeting key alteration minerals in epithermal deposits in Patagonia, Argentina, using ASTER imagery and principal component analysis: International Journal of Remote Sensing, **24**, 4233–4240, doi: 10.1080/0143116031000152291.

Cunha, L. O., A. C. Dutra, and A. B. Costa, 2017, Use of radiogenic heat for demarcation of hydrothermal alteration zones in the Pernambuco-Brazil: Journal of Applied Geophysics, **145**, 111–123, doi: 10.1016/j.jappgeo.2017.08.004.

Czarnota, K., R. S. Blewett, and B. Goscombe, 2010, Predictive mineral discovery in the eastern Yilgarn Craton, Western Australia: an example of district scale targeting of an orogenic gold mineral system: Precambrian Research, **183**, 356–377, doi: 10.1016/j.precamres.2010.08.014.

Dentith, M., and S. T. Mudge, 2014, Geophysics for the mineral exploration geoscientist: Cambridge University Press.

Dopico, C. I. M., C. Lana, H. S. Moreira, L. F. Cassino, and F. F. Alkmim, 2017, U–Pb ages and Hf-isotope data of detrital zircons from the late Neoarchean–Paleoproterozoic Minas Basin, se Brazil: Precambrian Research, **291**, 143–161, doi: 10.1016/j.precamres.2017.01.026.

Endo, I., and F. Chamale Júnior, 1992, Modelo de evolução cinemática do sinclinal alegria e adjacências, quadrilátero ferrífero, mg: Revista Escola de Minas, **45**, 24–27.

Endo, I., C. E. R. Delgado, M. M. F. de Oliveira, A. d. C. Zapparoli, D. U. Carlos, H. F. Galbiatti, P. d. T. A. Castro, M. T. d. F. Suita, M. S. C. Barbosa, C. E. Lana, and L. G. B. d. Moura, 2019, Estratigrafia e arcabouço estrutural do quadrilátero ferrífero: Nota explicativa do mapa geológico do quadrilátero ferrífero, Minas Gerais, Brasil: Technical report, Departamento de Geologia, Escola de Minas – UFOP, Centro de Estudos Avançados do Quadrilátero Ferrífero, Ouro Preto, MG, Brazil. (Escala 1:150,000).

Evjen, H. M., 1936, The place of the vertical gradient in gravitational interpretations: Geophysics, **1**, 127–136, doi: 10.1190/1.1437067.

Fabricio-Silva, W., H. E. Frimmel, M. E. Shutesky, C. A. Rosière, and A. J. Massucatto, 2021, Temperature-controlled ore evolution in orogenic gold systems related to synchronous granitic magmatism: An example from the iron quadrangle province, Brazil: Economic Geology, **116**, 937–962, doi: 10.5382/econgeo.4814.

Fabricio-Silva, W., C. A. Rosière, and B. Bühn, 2019, The shear zone-related gold mineralization at the turmalina deposit, quadrilátero ferrífero, Brazil: Structural evolution and the two stages of mineralization: Mineralium Deposita, **54**, 347–368, doi: 10.1007/s00126-018-0811-7.

Farina, F., C. Albert, C. M. Dopico, C. A. Gil, H. Moreira, J. P. Hippertt, K. Cutts, F. F. Alkmim, and C. Lana, 2016, The archean–paleoproterozoic evolution of the Quadrilátero Ferrífero (Brasil): Current models and open questions: Journal of South American Earth Sciences, **68**, 4–21, doi: 10.1016/j.jsames.2015.10.015.

Farina, F., C. Albert, and C. Lana, 2015, The neoarchean transition between medium- and high-K granitoids: Clues from the Southern são Fran-

cisco Craton (Brazil): Precambrian Research, **266**, 375–394, doi: 10.1016/j.precamres.2015.05.038.

Ferreira, F. J. F., 1991, Aerogamaespectrometria e aeromagnetometria de um trato ocidental do précambriano paulista: PhD thesis, Instituto de Geociências, Universidade de São Paulo, São Paulo, Brazil. (150 p.).

Ford, A., K. J. Peters, G. A. Partington, P. L. Blevin, P. M. Downes, J. A. Fitzherbert, and J. E. Greenfield, 2019, Translating expressions of intrusion-related mineral systems into mappable spatial proxies for mineral potential mapping: Case studies from the southern new england orogen, australia: Ore Geology Reviews, **111**, 102943, doi: 10.1016/j.oregeorev.2019.102943.

Goldfarb, R. J., and D. I. Groves, 2015, Orogenic gold: Common or evolving fluid and metal sources through time: Lithos, **233**, 2–26, doi: 10.1016/j.lithos.2015.07.011.

Groves, D. I., M. Santosh, J. Deng, Q. Wang, L. Yang, and L. Zhang, 2020, A holistic model for the origin of orogenic gold deposits and its implications for exploration: Mineralium Deposita, **55**, 275–292, doi: 10.1007/s00126-019-00877-5.

Hagemann, S. G., V. A. Lisitsin, and D. L. Huston, 2016, Mineral system analysis: Quo vadis: Ore Geology Reviews, **76**, 504–522, doi: 10.1016/j.oregeorev.2015.12.012.

Harris, J. R., L. Wilkinson, K. Heather, S. Fumerton, M. A. Bernier, J. Ayer, and R. Dahn, 2001, Application of gis processing techniques for producing mineral prospectivity maps—a case study: mesothermal au in the swayze greenstone belt, ontario, canada: Natural Resources Research, **10**, 91–124, doi: 10.1023/A:1011548709573.

Hartmann, L. A., I. Endo, M. T. F. Suita, J. O. S. Santos, J. C. Frantz, M. A. Carneiro, N. J. McNaughton, and M. E. Barley, 2006, Provenance and age delimitation of quadrilátero ferrífero sandstones based on zircon u–pb isotopes: Journal of South American Earth Sciences, **20**, 273–285, doi: 10.1016/j.jsames.2005.07.015.

Herbert, S., T. Woldai, E. J. M. Carranza, and F. J. van Ruitenbeek, 2014, Predictive mapping of prospectivity for orogenic gold in uganda: Journal of African Earth Sciences, **99**, 666–693, doi: 10.1016/j.jafrearsci.2014.03.001.

Holden, E. J., J. C. Wong, P. Kovesi, D. Wedge, M. Dentith, and L. Bagas, 2012, Identifying structural complexity in aeromagnetic data: An image analysis approach to greenfields gold exploration: Ore Geology Reviews, **46**, 47–59, doi: 10.1016/j.oregeorev.2011.11.002.

Koglin, N., A. Zeh, A. R. Cabral, A. A. S. Gomes Jr, A. V. C. Neto, W. J. Brunetto, and H. Galbiatti, 2014, Depositional age and sediment source of the auriferous moeda formation, quadrilátero ferrífero of Minas Gerais, Brazil: New constraints from u–pb–hf isotopes in zircon and xenotime: Precambrian Research, **255**, 96–108, doi: 10.1016/j.precamres.2014.09.010.

Lana, C., F. F. Alkmim, R. Armstrong, R. Scholz, R. Romano, and H. A. Nalini Jr, 2013, The ancestry and magmatic evolution of archaean ttg rocks of the quadrilátero ferrífero province, southeast Brazil: Precambrian Research, **231**, 157–173, doi: 10.1016/j.precamres.2013.03.008.

Leite, E. P., and C. R. de Souza Filho, 2009, Artificial neural networks applied to mineral potential mapping for copper–gold mineralizations in the carajás mineral province, Brazil: Geophysical Prospecting, **57**, 1049–1065, doi: 10.1111/j.1365-2478.2008.00779.x.

Lobato, L. M., L. C. Ribeiro-Rodrigues, and F. W. R. Vieira, 2001a, Brazil's premier gold province. part ii: geology and genesis of gold deposits in the archean rio das velhas greenstone belt, quadrilátero ferrífero: Mineralium Deposita, **36**, 249–277, doi: 10.1007/s001260100180.

Lobato, L. M., L. C. Ribeiro-Rodrigues, M. Zucchetti, C. M. Noce, O. F. Baltazar, L. C. da Silva, and C. P. Pinto, 2001b, Brazil's premier gold province. part i: The tectonic, magmatic, and structural setting of the archean rio das velhas greenstone belt, quadrilátero ferrífero: Mineralium Deposita, **36**, 228–248.

Marinho, M. S., J. R. Magalhães, J. C. Lombello, J. Araújo, L. P. P. Di Salvio, R. N. Silva, D. C. Brito, W. L. Feboli, and C. F. Basto, 2023, Stratigraphy of the pitangui synclinorium, northwest of the quadrilátero ferrífero mineral province-Brazil: magmatism and sedimentation from archean to neoproterozoic: Journal of the Geological Survey of Brazil, **6**, 135–164, doi: 10.29396/jgsb.

Marinho, M. S., M. A. Silva, J. C. Lombello, L. P. Disalvio, R. N. Silva, W. L. Féboli, and D. C. Brito, 2018, Projeto arim - áreas de relevante interesse mineral – noroeste do quadrilátero ferrífero – mapa geológico integrado do sinclinório pitangui. (1 mapa colorido, escala 1:75.000. Access on: May 23, 2022, https://rigeo.cprm.gov.br/handle/doc/17219).

Maurer, V. C., G. H. C. de Melo, C. de Carvalho Lana, M. de Souza Marinho, S. P. V. Batista, L. M. da Silveira, G. Queiroga, M. P. Castro, and M. Silva, 2021, Trace elements in pyrite and pyrrhotite in the pitangui orogenic au deposit, pitangui greenstone belt, são francisco craton: Implications for the ore-forming fluids and metal sources: Journal of South American Earth Sciences, **111**, 103459, doi: 10.1016/j.jsames.2021.103459.

McCuaig, T. C., S. Beresford, and J. Hronsky, 2010, Translating the mineral systems approach into an effective exploration targeting system: Ore Geology Reviews, **38**, 128–138, doi: 10.1016/j.oregeorev.2010.05.008.

McCuaig, T. C., and J. M. Hronsky, 2014, The mineral system concept: the key to exploration tar-

geting, *in* Society of Economic Geologists Special Publication: **18**, 153–175. doi: 10.5382/SP.18.08.

Miller, H. G., and V. Singh, 1994, Potential field tilt—a new concept for location of potential field sources: Journal of Applied Geophysics, **32**, 213–217, doi: 10.1016/0926-9851(94)90022-1.

Nabighian, M. N., 1972, The analytic signal of two-dimensional magnetic bodies with polygonal cross-section: its properties and use for automated anomaly interpretation: Geophysics, **37**, 507–517, doi: 10.1190/1.1440276.

Nabighian, M. N., 1974, Additional comments on the analytic signal of two-dimensional magnetic bodies with polygonal cross-section: Geophysics, **39**, 85–92, doi: 10.1190/1.1440416.

Pires, A. C. B., 1995, Identificação geofísica de áreas de alteração hidrotermal, crixás-guarinos, goiás: Brazilian Journal of Geology, **25**, 61–68, doi: 10.25249/0375-7536.19956168.

Ribeiro, B. O. L., D. Barbuena, and G. H. C. de Melo, 2023, Geochemical multifractal modeling of soil and stream sediment data applied to gold prospectivity mapping of the Pitangui Greenstone Belt, northwest of Quadrilátero Ferrífero, Brazil: Geochemistry, **83**, 125951, doi: 10.1016/j.chemer.2023.125951.

Ribeiro, L. M. A. L., and O. F. Baltazar, 2013, Carta geológica: folha igarapé, SF.23-X-A-I. (Scale 1:100.000).

Ribeiro, V. B., M. Mantovani, and V. H. A. Louro, 2014, Aerogamaespectrometria e suas aplicações no mapeamento geológico: Terræ Didática, **10**, 29–51, doi: 10.20396/td.v10i1.8637386.

Ribeiro, V. B., and M. S. M. Mantovani, 2016, Gamma spectrometric and magnetic interpretation of Cabaçal copper deposit in mato grosso (Brazil): Implications for hydrothermal fluids remobilization: Journal of Applied Geophysics, **135**, 223–231, doi: 10.1016/j.jappgeo.2016.10.016.

Roest, W. R., J. Verhoef, and M. Pilkington, 1992, Magnetic interpretation using the 3-D analytic signal: Geophysics, **57**, 116–125, doi: 10.1190/1.1443174.

Romano, A. W., 2007, Geologia da folha Pará de Minas SE.23-Z-C-IV. (Scale 1:100.000).

Romano, R., C. Lana, F. F. Alkmim, G. Stevens, and R. Armstrong, 2013, Stabilization of the southern portion of the São Francisco craton, SE Brazil, through a long-lived period of potassic magmatism: Precambrian Research, **224**, 143–159, doi: 10.1016/j.precamres.2012.09.002.

Romano, R. W., J. C. S. Araújo, H. R. S. Carvalho, J. A. de Oliveira, M. G. Lemos, L. G. Knauer, C. T. Paiva, and C. A. Heineck, 2009, Geologia e recursos minerais da folha Contagem, SE.23-Z-C-V. (Scale 1:100.000).

Schodde, R., 2017, Recent trends and outlook for global exploration. (Conference presentation, Prospectors and Developers Association of Canada Convention, Toronto, 47.).

Silva, M. A., C. A. Pinto, M. A. P. Pinheiro, M. S. Marinho, J. C. Lombello, J. M. M. P. Pinho, L. E. A. Goulart, and J. R. Magalhães, 2020, Mapa Geológico do Estado de Minas Gerais. (Access on: May 23, 2022, https://rigeo.cprm.gov.br/handle/doc/21828).

Soares, M. B., A. V. Corrêa Neto, L. C. Bertolino, F. E. A. Alves, A. M. de Almeida, P. H. M. da Silva, R. O. A. Mabub, L. G. Manduca, and I. M. C. de Pamplona Araújo, 2018, Multistage mineralization at the hypozonal São Sebastião gold deposit, Pitangui greenstone belt, Minas Gerais, Brazil: Ore Geology Reviews, **102**, 618–638, doi: 10.1016/j.oregeorev.2018.09.028.

Soares, M. B., A. V. Corrêa Neto, and W. Fabricio-Silva, 2020, The development of a meso- to neoarchean rifting-convergence-collision-collapse cycle over an ancient thickened protocontinent in the south são francisco craton, Brazil: Gondwana Research, **77**, 40–66, doi: 10.1016/j.gr.2019.06.017.

Soares, M. B., A. V. C. Neto, A. Zeh, A. R. Cabral, L. F. Pereira, M. G. B. do Prado, and T. M. Schlichta, 2017, Geology of the Pitangui greenstone belt, Minas Gerais, Brazil: stratigraphy, geochronology and BIF geochemistry: Precambrian Research, **291**, 17–41, doi: 10.1016/j.precamres.2017.01.008.

Soares, M. B., D. Selby, L. Robb, and A. V. Corrêa Neto, 2021, Sulfide recrystallization and gold remobilization during the 2.0 Ga stage of the Minas orogeny: implications for gold mineralization in the Quadrilátero Ferrífero area, Brazil: Economic Geology, **116**, 1455–1466, doi: 10.5382/econgeo.4830.

Souza Filho, C. R., A. R. Nunes, E. P. Leite, L. V. S. Monteiro, and R. P. Xavier, 2007, Spatial analysis of airborne geophysical data applied to geological mapping and mineral prospecting in the Serra Leste region, Carajás Mineral Province, Brazil: Surveys in Geophysics, **28**, 377–405, doi: 10.1007/s10712-008-9031-5.

Tassinari, C. C., A. M. Mateus, M. E. Velásquez, J. M. Munhá, L. M. Lobato, R. M. Bello, A. P. Chiquini, and W. F. Campos, 2015, Geochronology and thermochronology of gold mineralization in the Turmalina deposit, NE of the Quadrilátero Ferrífero region, Brazil: Ore Geology Reviews, **67**, 368–381, doi: 10.1016/j.oregeorev.2014.12.013.

Ribeiro, B.O.L.: Conceptualization, Methodology, Formal Analysis and Investigation, Writing - Original draft preparation; **Barbuena, D.:** Writing - Original draft preparation, Writing - Review and Editing, Supervision; **de Melo, G.H.C.:** Writing - Original draft preparation, Writing - Review and Editing, Supervision.

Received on August 4, 2023 / Accepted on April 20, 2024